JACS
JOURNAL OF THE AMERICAN CHEMICAL SOCIETY
pubs.acs.org/JACS
Communication

A High-Performance Single-Molecule Magnet Utilizing Dianionic Aminoborolide Ligands

James C. Vanjak, Branford O. Wilkins, Veacheslav Vieru, Nattamai S. Bhuvanesh, Joseph H. Reibenspies, Caleb D. Martin, Liviu F. Chibotaru, and Michael Nippe*

Cite This: J. Am. Chem. Soc. 2022, 144, 17743−17747
Read Online
ACCESS | Metrics & More | Article Recommendations | Supporting Information

ABSTRACT: The first example of a homoleptic f-block borolide sandwich complex is presented and shown to be a high-performance single-molecule magnet (SMM). The bis(borolide) complex [K(2.2.2)][[1-(piperidino)-2,3,4,5-tetraphenylborolyl]$_2$Dy] (**1**) features an unusual example of an anionic Ln^{3+} metallocene that supports short metal−ligand bonds and a high degree of linearity around the central Dy^{3+} ion, resulting in comparatively large barriers to magnetization reversal (U_{eff} = 1600 cm^{-1} for the most linear orientation) and, importantly, a high blocking temperature (T_B, defined as $T(\tau_{100s})$) of 66 K. These metrics put complex **1** among the very best performing SMMs reported to date and highlight the potential of dianionic borolide ligands to increase ligand field axiality, compared to monoanionic cyclic ligands, to ultimately maximize magnetic anisotropy in f-block-based SMMs.

The design of single-molecule magnets (SMMs) that are amenable to practical applications such as ultrahigh-density data storage, quantum information processing, and molecular spintronics has progressed immensely with the discovery of lanthanide (Ln)-based SMMs.[1−5] Ln^{3+} ions are especially suited for SMM design, for they possess intrinsically strong anisotropic electron densities that can be complemented by careful modulation of the ligand field.[6−8] This ability to tailor ligand fields to afford specific magnetic properties is aptly shown by the trailblazing dysprosocenium family of sandwich complexes, sporting blocking temperatures ($T(\tau_{100s})$) of up to 65 K,[9−12] approaching the boiling point of N_2. These attributes stem from tuning of the interplay of electrostatic interactions between the Cp^R−Dy (Cp^R = substituted cyclopentadienide ligands shown in Chart 1) distance and the Cp^R−Dy−Cp^R angle to enforce a rigid and highly axial ligand field on the oblate electron density of the Dy^{3+} ion. Functionalization of the Cp^R rings has not only allowed *(i)* maximization of the axiality, which mitigates the efficacy of undesired through-barrier relaxation pathways such as quantum tunneling of the magnetization (QTM) and increases the energy gap between the magnetic ground- and excited-state multiplets, thereby maximizing the effective energy barrier to magnetization reversal (U_{eff}), but also *(ii)* alteration of vibrational modes that reduce the blocking temperature via spin−vibrational coupling. Recent calculations suggest that the performance of dysprosocenium SMMs could be even further improved via encapsulation into SWCNTs.[13]

While the Cp^{R-} ligand platform has enabled a plethora of organometallic f-block chemistry and has been intimately involved in SMM design, given the largely ionic character of 4f−ligand bonding, the monoanionic charge of Cp^{R-} may present an electrostatic limit on how strong the ligand field can become. As a new avenue to improve SMM performance, we commenced an exploration of dianionic ligands that can furnish highly axial ligand fields for 4f complexes and identified aminoborolides as promising candidates. Borolides in general are isoelectronic dianionic analogues of cyclopentadienides and allow for comparable tunability of the ligand framework to enforce appropriate steric bulk.[14] The multiconfigurational electronic structure that aminoborolides have been shown to possess, namely, resonance forms involving transition metal−ligand redox events, make them uniquely suited for the design of high-performance Ln SMMs.[14] While the metal-reduced resonance structures have been shown not to reduce Ln^{3+} ions (vide infra), their presence places greater electron density at the Ln^{3+} ion, enhancing electrostatic interactions.[14] In contrast to the precedence of Ln complexes bearing five-membered

Chart 1. Comparison of Magnetic and Structural Characteristics of Dysprosocenium Complexes[9−12] and 1[a]

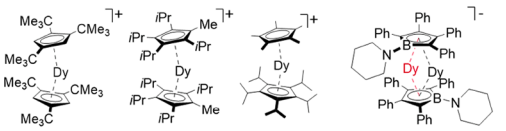

	a.	b.	c.	1_a, 1_b
$T(\tau_{100s})$	60 K	62 K	65 K	66 K, 60 K
d(Dy-$Ring_c$)	2.317[1]Å	2.298[5] Å	2.290[1] Å	2.259[6] Å, 2.269[6] Å
∠($Ring_c$-Dy-$Ring_c$)	152.845(2)°	156.6(3)°	162.507(1)°	161.4(3)°, 158.6(3)°

[a]The two sets of parameters for **1** ($\mathbf{1_a}$, $\mathbf{1_b}$) correspond to the two Dy^{3+} sites in crystalline material of **1**. The $T(\tau_{100s})$ value for $\mathbf{1_b}$ was extrapolated from the Orbach term only (vide infra).

Received: June 25, 2022
Published: September 26, 2022

https://doi.org/10.1021/jacs.2c06698
J. Am. Chem. Soc. 2022, 144, 17743−17747

heterocycles such as arsolyls,[15,16] phospholyls,[16−18] and pyrollyls[19] as well as six-membered heterocycles like phosphorins,[20] boratabenzenes,[21] and 5f complexes of borabenzene,[22] Ln sandwich complexes of aminoborolides have not been reported to date, and only recently have the magnetic properties of a heteroleptic benzoborole−COT Dy^{3+} complex been investigated.[23] Here we report the synthesis of the new aminoborolide ligand **3** and its corresponding anionic homoleptic Dy^{3+} sandwich complex **1**, which shows a high $T(\tau_{100s})$ rivaling those of its cationic dysprosocenium congeners.

The reaction of piperidino(dichloro)borane (**5**)[24] with dilithiotetraphenylbutadienide (**6**)[25] affords the new 1-piperidino-2,3,4,5-tetraphenylborole **4** as an air-stable solid in 68% yield (Scheme 1). The short B−N distance of 1.396(3) Å

Scheme 1. Synthetic Route to 1

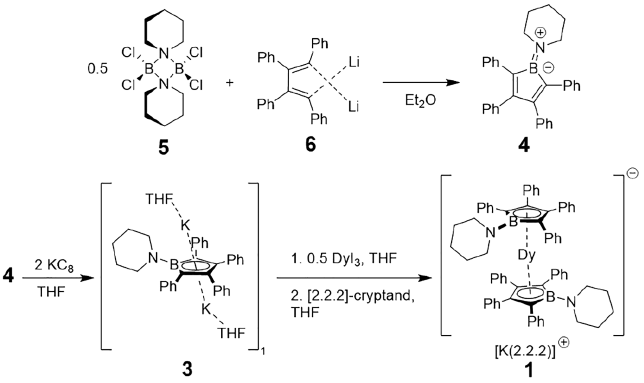

in the crystal structure of **4** (see the Supporting Information (SI)) and the ν(BN) stretching frequency of 1484 cm^{-1} implies a major contribution of the azaborafulvene resonance structure to the ground state of **4**.[26,27] Facile two-electron reduction of **4** with potassium graphite yields air-sensitive $[K(THF)]_2$[1-(piperidino)-2,3,4,5-tetraphenylborolide] (**3**) in 88% yield. A longer B−N distance of 1.48(2) Å and smaller ν(BN) stretching frequency of 1471 cm^{-1} are observed for **3** compared to **4**. This is consistent with previous reports and attributed to population of the B═N π^* LUMO upon reduction, reducing the bond order to a single bond in **3**.[26−28] The salt metathesis reaction between **3** and THF-solvated DyI_3 allows ready access to the anionic homoleptic sandwich complex **2** in 53% yield, which was unambiguously established as $[K(THF)_6]$[1-(piperidino)-2,3,4,5-tetraphenylborolyl]$_2$Dy by means of single-crystal X-ray diffraction[29] (see the SI for details). However, these crystals suffer greatly from desolvation at room temperature, which renders reproducible magnetic measurements infeasible. To alleviate this issue, [2.2.2]-cryptand is added to **2** to furnish air-sensitive [K(2.2.2)][1-(piperidino)-2,3,4,5-tetraphenylborolyl]$_2$Dy (**1**) in 33% yield, which is devoid of detectable desolvation at room temperature.

The molecular structure of **1** (Figure 1) features the anticipated anionic homoleptic sandwich complex. Closer inspection revealed elongated thermal ellipsoids of several atoms, most importantly the Dy^{3+} ions, indicative of structural disorder within the crystalline material. Crystallization from alternative solvent mixtures and crystallization at −32 °C yielded crystalline materials that possessed similar disorder at the metal site. The disorder in **1** was modeled and successfully refined assuming disorder of the Dy^{3+} ion over two positions.

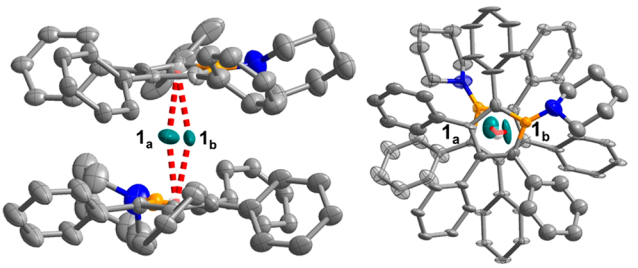

Figure 1. Molecular structure of **1**, with thermal ellipsoids drawn at the 25% probability level. Dy = teal, B = gold, N = blue, C = gray. The countercation and hydrogens have been omitted for clarity.

Site $\mathbf{1}_a$ features a $TPhBN_c$−Dy−$TPhBN_c$ ($TPhBN_c$ = borolide ring centroid) angle of 161.4(3)° and $TPhBN_c$−Dy distances of 2.274(6) and 2.244(6) Å, while site $\mathbf{1}_b$ possesses a less linear $TPhBN_c$−Dy−$TPhBN_c$ angle of 158.6(3)° and slightly longer $TPhBN_c$−Dy distances of 2.258(6) and 2.280(5) Å. These structural metrics are comparable to those reported for dysprosocenium ions in $[(Cp^*)Dy(Cp^{iPr_5})][B(C_6F_5)_4]$ ($Cp^{iPr_5}{}_c$−Dy−$Cp^*{}_c$ angle of 162.507(1)° and Dy−$Cp^*{}_c$ and Dy−$Cp^{iPr_5}{}_c$ distances of 2.296(1) and 2.284(1) Å)[12] and $[Dy(Cp^{iPr_4Me})_2][B(C_6F_5)_4]$ ($Cp^{iPr_4Me}{}_c$−Dy−$Cp^{iPr_4Me}{}_c$ angle of 156.6(3)°, Dy−$Cp^{iPr_4Me}{}_c$ distances of 2.298(5) Å).[11]

The temperature dependence of the static magnetic properties of **1** were probed using direct current (dc) magnetic susceptibility measurements under an applied field of 1000 Oe in the temperature range of 2−300 K (Figure S15). The $\chi_M T$ value of 14.30 emu K mol^{-1} at 300 K is close to the expected value for a single noninteracting Dy^{3+} ion (14.17 emu K mol^{-1}: $^6H_{15/2}$, $S = {}^5/_2$, $L = 5$, $g = {}^4/_3$). Field-cooled (FC) and zero-field-cooled (ZFC) magnetization data show clear divergence at 68 K, indicative of magnetic blocking. The dynamic magnetic properties of **1** were initially probed by means of alternating current (ac) magnetometry in the temperature range of 74 to 116 K. The out-of-phase component of the ac magnetic susceptibility χ'' (Figure 2a) features two peaks, indicative of two distinct relaxation processes and consistent with the presence of two independent Dy^{3+} sites in **1**. Temperature-dependent relaxation times τ (Figure 2c) were extracted from fits of Cole−Cole plots that bear both processes in the frequency window (Figure S17, 80−104 K) to a two-process generalized Debye model as implemented within the CC-FIT2 software package[30,31] (open circles).

At temperatures below 76 K, both relaxation processes are too slow to display maxima in χ'' above the 0.1 Hz low-frequency instrument limit. Variable-temperature magnetization decay experiments (Figures S16−S27) were carried out to extend the temperature range over which the temperature dependence of the magnetic relaxation could be studied. Structural disorder likely remains in crystalline material of **1** below 76 K, and therefore, two independent relaxation processes are expected to contribute over this temperature regime. However, the use of double-stretched exponential fits did not provide statistically meaningful results; hence, we provide τ values resulting from a single-stretched exponential fitting procedure (CC-FIT2),[30] which yielded the most conservative estimate for bulk relaxation in crystalline material of **1** (triangles in Figure 2c). The thus-obtained τ values of the bulk sample are well-aligned with those obtained from ac measurements for the slower process in the higher-temperature regime. The temperature dependence of the ac-

https://doi.org/10.1021/jacs.2c06698
J. Am. Chem. Soc. 2022, 144, 17743−17747

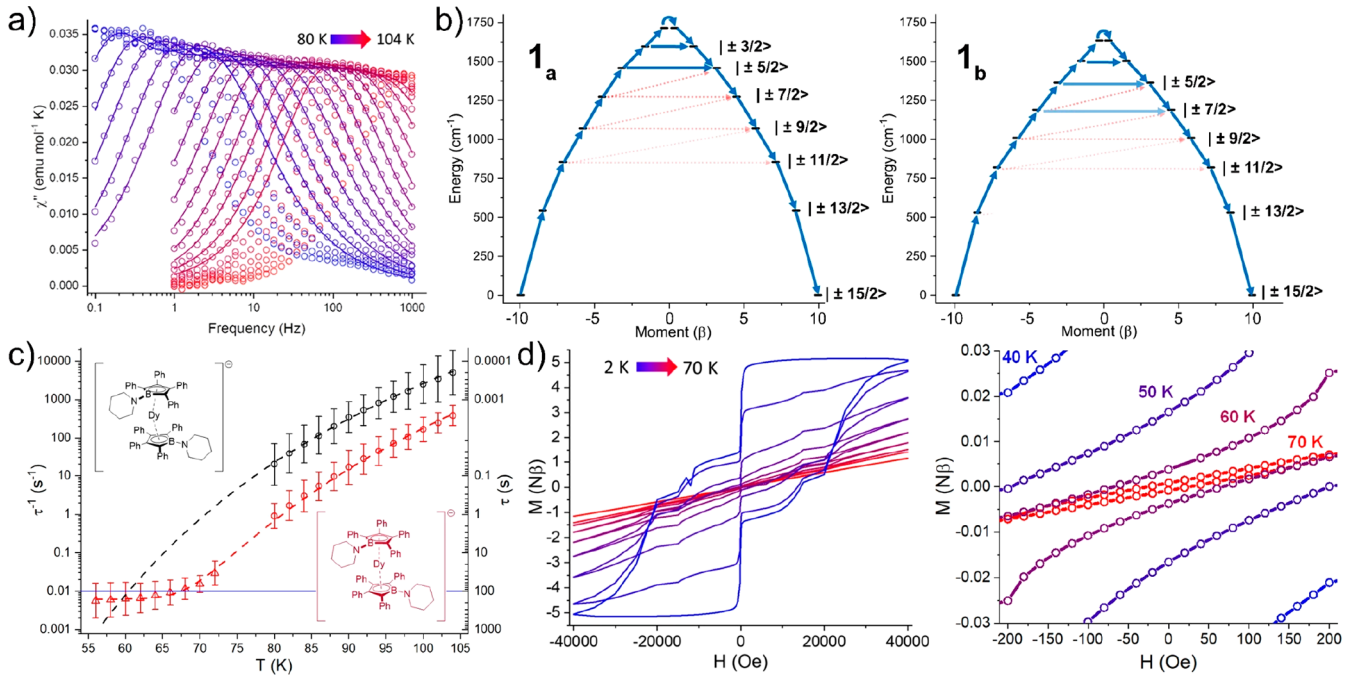

Figure 2. (a) Out-of-phase component of the molar ac magnetic susceptibility of **1** (H_{dc} = 0 Oe). Circles represent experimental data, and lines correspond to fits. (b) Ab initio-calculated energies of excited magnetic states (labels indicate major contributions) and most probable relaxation pathways (blue arrows) for (left) $\mathbf{1}_a$ and (right) $\mathbf{1}_b$ (see Figure S4 and Table S7 for all transition probabilities).[32] (c) Temperature dependence of the relaxation times for $\mathbf{1}_a$ (red) and $\mathbf{1}_b$ (black) in **1** extracted from fits of Cole−Cole plots (circles) or magnetization decay experiments (triangles). The slower and faster relaxation processes were fit using the Orbach and Raman terms (red dashed line) and the Orbach term only (black dashed line), respectively. $T(\tau_{100s})$ is highlighted by the blue line. (d) (left) Variable-field magnetization data for **1** from 2 to 70 K obtained for a sweep rate of 9 Oe s^{-1}. (right) Magnification of hysteresis loops at selected temperatures. The 70 K loop can be considered closed.

and dc-derived relaxation times for the slower process in Figure 2b (red) was fitted according to the relaxation rate equation shown in eq 1,

$$\tau^{-1} = CT^n + \tau_0^{-1} e^{-U_{eff}/k_B T} \quad (1)$$

which is truncated to include only the Orbach (τ_0, U_{eff}) and Raman (C, n) terms. The fit afforded the values U_{eff} = 1600 ± 100 cm^{-1}, $\tau_0 = (1 \pm 2) \times 10^{-12}$ s, $C = 0 \pm 0.2$ s^{-1} K^{-n}, and $n = 0 \pm 7$ for $\mathbf{1}_a$. The rather large errors are a result of including simple fitting errors according to eq 1, 1σ uncertainties in the ac-derived relaxation times from the log-normal distribution model, and uncertainties associated with the distribution factors α and β values for ac- and dc-extracted relaxation times, respectively. Exclusion of the latter during error analysis results in significantly smaller errors (U_{eff} = 1658 ± 2 cm^{-1}, $\tau_0 = (2.01 \pm 0.07) \times 10^{-13}$ s, $C = (2.4 \pm 0.1) \times 10^{-6}$ s^{-1} K^{-n}, and n = 1.93 ± 0.02). The faster process was fitted using its corresponding ac-derived relaxation times to solely an Orbach process to afford U_{eff} = 1300 ± 300 cm^{-1} and $\tau_0 = (2 \pm 8) \times 10^{-12}$ s.

With these results in mind, we assign the more and less linear sites $\mathbf{1}_a$ and $\mathbf{1}_b$ to the slower and faster relaxation processes, respectively. Based on the established temperature dependences of τ, we extract blocking temperatures $T(\tau_{100s})$ of 67 K for site $\mathbf{1}_a$ and 60 K for site $\mathbf{1}_b$. However, given the mentioned experimental errors, we suggest that 66 K be used as the more conservative estimate for the blocking temperature of site $\mathbf{1}_a$ (τ_{dc}(66 K) = 108 ± 0.4 K), which is close to that reported for a heteroleptic dysprosocenium complex (65 K).[12]

To understand the origin of the slower and faster relaxation processes, ab initio calculations of the CASSCF/SO-RASSI/SINGLE_ANISO type were carried out with the OpenMolcas program for sites $\mathbf{1}_a$ and $\mathbf{1}_b$.[32−34] Figure 2b summarizes the results of these calculations. The calculated energy ordering of the ground and excited states of sites $\mathbf{1}_a$ and $\mathbf{1}_b$ and the corresponding transition probabilities are in good agreement with the experimental data. Considering solely the matrix elements connecting the corresponding states, the more linear site $\mathbf{1}_a$ and the less linear site $\mathbf{1}_b$ are calculated to relax via the fifth excited state (at 1458 and 1367 cm^{-1}, respectively). However, at high temperature the temperature-assisted tunneling (TAT) mechanism dominates the relaxation, with the probability of relaxation given by $\mathcal{P}_n = \mu^2 e^{-E_n/k_B T}$, where μ is the average magnetic moment matrix element connecting the opposite components of the corresponding doublet, E_n is the energy of doublet n, and k_B is the Boltzmann constant. Using the ab initio-calculated energies and the corresponding matrix elements, we obtain $\frac{\mathcal{P}_{-6\rightarrow+6}}{\mathcal{P}_{-5\rightarrow+5}} = 7.4$ at 60 K. This implies that activated relaxation via the sixth excited state (1595 cm^{-1} for $\mathbf{1}_a$) dominates over the one via the fifth excited state (1458 cm^{-1}) at this temperature. These calculated energies are in very good agreement with the experimentally determined barriers U_{eff} = 1600 and 1300 cm^{-1}. Thus, in the case of **1**, computational results support differences in electronic structure between $\mathbf{1}_a$ and $\mathbf{1}_b$ causing the slower and faster relaxation processes observed in bulk crystalline material. This is in contrast to a recent report of a dysprosium metallocene SMM in which two disordered Dy^{3+} sites featured almost identical magnetic state energy ordering and transition probabilities yet varying relaxation rates.[35]

Magnetic hysteresis measurements further highlight the magnetic anisotropy of **1** in bulk crystalline material. As shown

https://doi.org/10.1021/jacs.2c06698
J. Am. Chem. Soc. 2022, 144, 17743−17747

in Figure 2d, hysteresis loops gradually close from 2 to 70 K, at which point they are effectively closed. Complex **1** possesses a coercive field (H_c) of 7.5 Oe at 65 K, which is in agreement with the $T(\tau_{100s})$ of 66 K for $\mathbf{1_a}$. The sharp step at zero field could be attributed to the presence of QTM, likely originating from less linear Dy^{3+} sites in the bulk sample. We note that the increased ligand field strength of the dianionic borolide ligand may exacerbate the effects of deviations from geometric linearity on the magnetic properties. This ultimately leads to the introduction of additional relaxation pathways[36] as well as transverse magnetic anisotropy.[6,7]

In conclusion, we have shown that dianionic borolide ligands can exert strong ligand fields on trivalent lanthanide ions, resulting in remarkable magnetic anisotropy in the first 4f bis(borolide) sandwich complex **1**. The high axiality in $\mathbf{1_a}$ affords a very high blocking temperature. These proof-of-principle results open up additional routes to increase the performance of SMMs and to push blocking temperatures well above the boiling point of N_2 in the future. Such work is currently ongoing in our laboratories.

■ ASSOCIATED CONTENT

Supporting Information

The Supporting Information is available free of charge at https://pubs.acs.org/doi/10.1021/jacs.2c06698.

Experimental and computational details, additional magnetic data, fit parameters, and crystallographic details (PDF)

Accession Codes

CCDC 2181899−2181901 contain the supplementary crystallographic data for this paper. These data can be obtained free of charge via www.ccdc.cam.ac.uk/data_request/cif, or by emailing data_request@ccdc.cam.ac.uk, or by contacting The Cambridge Crystallographic Data Centre, 12 Union Road, Cambridge CB2 1EZ, U.K.; fax: +44 1223 336033.

■ AUTHOR INFORMATION

Corresponding Author

Michael Nippe − *Department of Chemistry, Texas A&M University, College Station, Texas 77843, United States;* orcid.org/0000-0003-1091-4677; Email: nippe@chem.tamu.edu

Authors

James C. Vanjak − *Department of Chemistry, Texas A&M University, College Station, Texas 77843, United States*

Branford O. Wilkins − *Department of Chemistry, Texas A&M University, College Station, Texas 77843, United States*

Veacheslav Vieru − *Maastricht Science Programme, Faculty of Science and Engineering, Maastricht University, 6229 EN Maastricht, The Netherlands*

Nattamai S. Bhuvanesh − *Department of Chemistry, Texas A&M University, College Station, Texas 77843, United States*

Joseph H. Reibenspies − *Department of Chemistry, Texas A&M University, College Station, Texas 77843, United States*

Caleb D. Martin − *Department of Chemistry and Biochemistry, Baylor University, Waco, Texas 76798, United States;* orcid.org/0000-0001-9681-0160

Liviu F. Chibotaru − *Theory of Nanomaterials Group, Katholieke Universiteit Leuven, 3001 Leuven, Belgium;* orcid.org/0000-0003-1556-0812

Complete contact information is available at: https://pubs.acs.org/10.1021/jacs.2c06698

Funding

We are grateful to the Welch Foundation (M.N.: Grant A-1880; C.D.M.: Grant AA-1846) and the National Science Foundation (M.N.: Award CHE-1753014; C.D.M.: Award 1753025) for their generous support of this work.

Notes

The authors declare no competing financial interest.

■ ACKNOWLEDGMENTS

We thank Dr. Sam Yruegas and Dr. Xiaojun Su for helpful discussions and synthetic advice.

■ REFERENCES

(1) Gatteschi, D.; Sessoli, R.; Villain, J. *Molecular Nanomagnets*; Oxford University Press: New York, 2006.

(2) Mannini, M.; Pineider, F.; Sainctavit, P.; Danieli, C.; Otero, E.; Sciancalepore, C.; Talarico, A. M.; Arrio, M.-A.; Cornia, A.; Gatteschi, D.; Sessoli, R. Magnetic memory of a single-molecule quantum magnet wired to a gold surface. *Nat. Mater.* **2009**, *8* (3), 194−197.

(3) Leuenberger, M. N.; Loss, D. Quantum computing in molecular magnets. *Nature* **2001**, *410* (6830), 789−793.

(4) Bogani, L.; Wernsdorfer, W. Molecular spintronics using single-molecule magnets. *Nat. Mater.* **2008**, *7* (3), 179−186.

(5) Ishikawa, N.; Sugita, M.; Ishikawa, T.; Koshihara, S.-y.; Kaizu, Y. Lanthanide Double-Decker Complexes Functioning as Magnets at the Single-Molecular Level. *J. Am. Chem. Soc.* **2003**, *125* (29), 8694−8695.

(6) Liu, J.-L.; Chen, Y.-C.; Tong, M.-L. Symmetry strategies for high performance lanthanide-based single-molecule magnets. *Chem. Soc. Rev.* **2018**, *47* (7), 2431−2453.

(7) Liddle, S. T.; van Slageren, J. Improving f-element single molecule magnets. *Chem. Soc. Rev.* **2015**, *44* (19), 6655−6669.

(8) Sorace, L.; Gatteschi, D.; Layfield, R. A.; Murugesu, M. *Lanthanides and Actinides in Molecular Magnetism*, 1st ed.; Wiley-VCH, 2015; pp 1−23.

(9) Goodwin, C. A. P.; Ortu, F.; Reta, D.; Chilton, N. F.; Mills, D. P. Molecular magnetic hysteresis at 60 K in dysprosocenium. *Nature* **2017**, *548* (7668), 439−442.

(10) Guo, F.-S.; Day, B. M.; Chen, Y.-C.; Tong, M.-L.; Mansikkamäki, A.; Layfield, R. A. A Dysprosium Metallocene Single-Molecule Magnet Functioning at the Axial Limit. *Angew. Chem., Int. Ed.* **2017**, *56* (38), 11445−11449.

(11) (a) McClain, K. R.; Gould, C. A.; Chakarawet, K.; Teat, S. J.; Groshens, T. J.; Long, J. R.; Harvey, B. G. High-temperature magnetic blocking and magneto-structural correlations in a series of dysprosium(III) metallocenium single-molecule magnets. *Chem. Sci.* **2018**, *9* (45), 8492−8503. (b) Gould, C. A.; McClain, K. R.; Reta, D.; Kragskow, J. G. C.; Marchiori, D. A.; Lachman, E.; Choi, E.-S.; Analytis, J. G.; Britt, R. D.; Chilton, N. F.; Harvey, B. G.; Long, J. R. Ultrahard magnetism from mixed-valence dilanthanide complexes with metal-metal bonding. *Science* **2022**, *375* (6577), 198−202.

(12) Guo, F.-S.; Day, B. M.; Chen, Y.-C.; Tong, M.-L.; Mansikkamäki, A.; Layfield, R. A. Magnetic hysteresis up to 80 K in a dysprosium metallocene single-molecule magnet. *Science* **2018**, *362* (6421), 1400−1403.

(13) Nabi, R.; Tiwari, R. K.; Rajaraman, G. *In silico* strategy to boost stability, axiality, and barrier heights in dysprocenium SIMs via SWCNT encapsulation. *Chem. Commun.* **2021**, *57* (86), 11350−11353.

(14) (a) Herberich, G. E.; Buller, B.; Hessner, B.; Oschmann, W. Derivative des borols: II. Pentaphenylborol: Synthese, reduktion zum dianion und komplexe von kobalt und platin. *J. Organomet. Chem.* **1980**, *195* (3), 253−259. (b) Herberich, G. E.; Hostalek, M.; Laven, R.; Boese, R. Borole Dianions: Metalation of 1-(Dialkylamino)-2,5-dihydro-l*H*-boroles and the Structure of $Li_2(C_4H_4BNEt_2)$·TMEDA. *Angew. Chem., Int. Ed. Engl.* **1990**, *29* (3), 317−318. (c) Jimenez-Halla, J. O. C.; Matito, E.; Solà, M.; Braunschweig, H.; Hörl, C.; Krummenacher, I.; Wahler, J. A theoretical study of the aromaticity in neutral and anionic borole compounds. *Dalton Trans.* **2015**, *44* (15), 6740−6747. (d) Braunschweig, H.; Breher, F.; Chiu, C.-W.; Gamon, D.; Nied, D.; Radacki, K. The Reduction Chemistry of Ferrocenylborole. *Angew. Chem., Int. Ed.* **2010**, *49* (47), 8975−8978. (e) Braunschweig, H.; Damme, A.; Gamon, D.; Kelch, H.; Krummenacher, I.; Kupfer, T.; Radacki, K. Synthesis, Coordination Behavior, and Reduction Chemistry of Cymantrenyl-1,3-bis(2,3,4,5-tetraphenyl)-borole. *Chem. - Eur. J.* **2012**, *18* (27), 8430−8436. (f) Yruegas, S.; Tang, H.; Bornovski, G. Z.; Su, X.; Sung, S.; Hall, M. B.; Nippe, M.; Martin, C. D. Nickel−Borolide Complexes and Their Complex Electronic Structure. *Inorg. Chem.* **2021**, *60* (21), 16160−16167.

(15) Nief, F.; Turcitu, D.; Ricard, L. Synthesis and structure of phospholyl- and arsolylthulium(II) complexes. *Chem. Commun.* **2002**, No. 15, 1646−1647.

(16) Mills, D. P.; Evans, P. f-Block Phospholyl and Arsolyl Chemistry. *Chem. - Eur. J.* **2021**, *27* (22), 6645−6665.

(17) Evans, P.; Reta, D.; Whitehead, G. F. S.; Chilton, N. F.; Mills, D. P. Bis-Monophospholyl Dysprosium Cation Showing Magnetic Hysteresis at 48 K. *J. Am. Chem. Soc.* **2019**, *141* (50), 19935−19940.

(18) Chen, S.-M.; Xiong, J.; Zhang, Y.-Q.; Yuan, Q.; Wang, B.-W.; Gao, S. A soft phosphorus atom to "harden" an erbium(III) single-ion magnet. *Chem. Sci.* **2018**, *9* (38), 7540−7545.

(19) Schumann, H.; Rosenthal, E. C. E.; Winterfeld, J.; Weimann, R.; Demtschuk, J. Organometallic compounds of the lanthanides. CIII Mixed sandwich complexes of the 4f elements: synthesis and crystal structure of (η^8-cyclooctatetraenyl)(η^5-2,5-di-*tert*-butylpyrrolyl)-samarium, -thulium, and -lutetium. *J. Organomet. Chem.* **1996**, *507* (1), 287−289.

(20) Arnold, P. L.; Cloke, F. G. N.; Hitchcock, P. B. The first structurally authenticated zerovalent heteroarene complex of a lanthanide; synthesis and X-ray structure of bis(2,4,6-tri-tert-butylphosphorin)holmium(0). *Chem. Commun.* **1997**, No. 5, 481−482.

(21) (a) Cui, P.; Chen, Y.; Zeng, X.; Sun, J.; Li, G.; Xia, W. Boratabenzene Derivatives of Divalent Samarium: Syntheses, Structures and Catalytic Reactivities of $(C_5H_5BXPh_2)_2Sm(THF)_2$ (X = N, P). *Organometallics* **2007**, *26* (26), 6519−6521. (b) Meng, Y.-S.; Wang, C.-H.; Zhang, Y.-Q.; Leng, X.-B.; Wang, B.-W.; Chen, Y.-F.; Gao, S. (Boratabenzene)(cyclooctatetraenyl) lanthanide complexes: a new type of organometallic single-ion magnet. *Inorg. Chem. Front.* **2016**, *3* (6), 828−835.

(22) Paprocki, V.; Hrobárik, P.; Harriman, K. L. M.; Luff, M. S.; Kupfer, T.; Kaupp, M.; Murugesu, M.; Braunschweig, H. Stable Actinide π Complexes of a Neutral 1,4-Diborabenzene. *Angew. Chem., Int. Ed.* **2020**, *59* (31), 13109−13115.

(23) Zhu, D.; Wang, M.; Guo, L.; Shi, W.; Li, J.; Cui, C. Synthesis, Structure, and Magnetic Properties of Rare-Earth Benzoborole Complexes. *Organometallics* **2021**, *40* (15), 2394−2399.

(24) Musgrave, O. C. The preparation of some dimeric sec.-Aminoboron dihalides. *J. Chem. Soc.* **1956**, 4305−4307.

(25) Fagan, P. J.; Manriquez, J. M.; Maatta, E. A.; Seyam, A. M.; Marks, T. J. Synthesis and properties of bis (pentamethylcyclopentadienyl) actinide hydrocarbyls and hydrides. A new class of highly reactive f-element organometallic compounds. *J. Am. Chem. Soc.* **1981**, *103* (22), 6650−6667.

(26) Niedenzu, K.; Dawson, J. W. Boron-Nitrogen Compounds. III.[1,2] Aminoboranes, Part 2: The BN Bond Character in Substituted Aminoboranes. *J. Am. Chem. Soc.* **1960**, *82* (16), 4223−4228.

(27) Gerrard, W.; Hudson, H.; Mooney, E. 995. Chemistry related to borazole. Part II. The reaction of secondary amines with boron trichloride. *J. Chem. Soc.* **1960**, 5168−5172.

(28) Heitkemper, T.; Sindlinger, C. P. Electronic Push−Pull Modulation by Peripheral Substituents in Pentaaryl Boroles. *Chem. - Eur. J.* **2019**, *25* (26), 6628−6637.

(29) Unit cell parameters for **2**: Triclinic, *P*1, a = 13.1182(16) Å, b = 16.088(2) Å, c = 21.442(3) Å, α = 68.130(4)°, β = 77.858(4)°, γ = 77.217(4)°, V = 4054.4(9) Å^3.

(30) Reta, D.; Chilton, N. F. Uncertainty estimates for magnetic relaxation times and magnetic relaxation parameters. *Phys. Chem. Chem. Phys.* **2019**, *21* (42), 23567−23575.

(31) Reta, D.; Chilton, N. F. Extraction of "hidden" relaxation times from AC susceptibility data. *Chem. Squared* **2020**, *4* (3), 1−9.

(32) Galván, I. F.; Vacher, M.; Alavi, A.; Angeli, C.; Aquilante, F.; Autschbach, J.; Bao, J. J.; Bokarev, S. I.; Bogdanov, N. A.; Carlson, R. K.; Chibotaru, L. F.; Creutzberg, J.; Dattani, N.; Delcey, M. G.; Dong, S. S.; Dreuw, A.; Freitag, L.; Frutos, L. M.; Gagliardi, L.; Gendron, F.; Giussani, A.; González, L.; Grell, G.; Guo, M.; Hoyer, C. E.; Johansson, M.; Keller, S.; Knecht, S.; Kovačević, G.; Källman, E.; Li Manni, G.; Lundberg, M.; Ma, Y.; Mai, S.; Malhado, J. P.; Malmqvist, P. Å.; Marquetand, P.; Mewes, S. A.; Norell, J.; Olivucci, M.; Oppel, M.; Phung, Q. M.; Pierloot, K.; Plasser, F.; Reiher, M.; Sand, A. M.; Schapiro, I.; Sharma, P.; Stein, C. J.; Sørensen, L. K.; Truhlar, D. G.; Ugandi, M.; Ungur, L.; Valentini, A.; Vancoillie, S.; Veryazov, V.; Weser, O.; Wesołowski, T. A.; Widmark, P.-O.; Wouters, S.; Zech, A.; Zobel, J. P.; Lindh, R. OpenMolcas: From Source Code to Insight. *J. Chem. Theory Comput.* **2019**, *15* (11), 5925−5964.

(33) Chibotaru, L. F.; Ungur, L. *Ab initio* calculation of anisotropic magnetic properties of complexes. I. Unique definition of pseudospin Hamiltonians and their derivation. *J. Chem. Phys.* **2012**, *137*, 064112.

(34) Ungur, L.; Thewissen, M.; Costes, J.-P.; Wernsdorfer, W.; Chibotaru, L. F. Interplay of Strongly Anisotropic Metal Ions in Magnetic Blocking of Complexes. *Inorg. Chem.* **2013**, *52* (11), 6328−6337.

(35) Guo, F.-S.; He, M.; Huang, G.-Z.; Giblin, S. R.; Billington, D.; Heinemann, F. W.; Tong, M.-L.; Mansikkamäki, A.; Layfield, R. A. Discovery of a Dysprosium Metallocene Single-Molecule Magnet with Two High-Temperature Orbach Processes. *Inorg. Chem.* **2022**, *61* (16), 6017−6025.

(36) Sottini, S.; Poneti, G.; Ciattini, S.; Levesanos, N.; Ferentinos, E.; Krzystek, J.; Sorace, L.; Kyritsis, P. Magnetic Anisotropy of Tetrahedral Co^{II} Single-Ion Magnets: Solid-State Effects. *Inorg. Chem.* **2016**, *55* (19), 9537−9548.

https://doi.org/10.1021/jacs.2c06698
J. Am. Chem. Soc. 2022, 144, 17743−17747